APPLIED GEOPHYSICS, Vol.18, No.1 (March 2021), P. 85–93, 10 Figures.
DOI:10.1007/s11770-021-0852-z

Multichannel deconvolution with spatial reflection regularization*

Li Hao[1,2], Li Guo-Fa*[1,2], Ma Xiong[1,2], Zhang Jia-Liang[3], Meng Qing-Long[3], and Zhang Zhu-Xin[3]

Abstract: Seismic deconvolution plays an important role in the seismic characterization of thin-layer structures and seismic resolution enhancement. However, the trace-by-trace processing strategy is applied and ignores the spatial connection along seismic traces, which gives the deconvolved result strong ambiguity and poor spatial continuity. To alleviate this issue, we developed a structurally constrained deconvolution algorithm. The proposed method extracts the reflection structure characterization from the raw seismic data and introduces it to the multichannel deconvolution algorithm as a spatial reflection regularization. Benefiting from the introduction of the reflection regularization, the proposed method enhances the stability and spatial continuity of conventional deconvolution methods. Synthetic and field data examples confirm the correctness and feasibility of the proposed method.
Keywords: Deconvolution, spatial reflection regularization, resolution, sparse-spike

Introduction

In reflection seismology, the recorded seismogram can be modeled as the convolution of a source wavelet with Earth reflectivity sequences (Lines and Ulrych, 1977). The major objective of seismic deconvolution is to remove the wavelet filtering effects from the recorded seismogram to obtain the ideal reflectivity sequences, which may be used to quantify seismic impedance mismatches between different geological layers (Gholami and Sacchi, 2012; de Figueiredo et al., 2014; Li, 2014). However, due to the band-limited nature of seismic wavelet, seismic deconvolution is an ill-posed problem that has countless results. To obtain a reasonable deconvolved result, incorporating as much prior knowledge about reflectivity as possible in the deconvolution algorithm is necessary. For example, with the assumption that the reflectivity sequences obey Gaussian distribution and the source wavelet has minimum phase, the well-known spiking deconvolution is developed using Wiener filtering (Berkhout, 1977). However, when the seismic wavelet is a mixed phase, the conventional spiking deconvolution cannot compress the seismic wavelet into an impulse, and the deconvolution result has the remaining phase.

Manuscript received by the Editor November 2, 2020; revised manuscript received March 22, 2021.
*This work was supported by National Key R & D Program of China (No.2018YFA0702504), the National Natural Science Foundation of China (Nos.42074141, 41874141) and the Strategic Cooperation Technology Projects of CNPC and CUP (ZLZX2020-03).
1. CNPC Key Laboratory of Geophysical Prospecting, China University of Petroleum, Beijing 102249, China
2. State Key Laboratory of Petroleum Resources and Prospecting, China University of Petroleum, Beijing 102249, China.
3. Dagang Oil Field, Petrochina, Tianjin 300280, China.
♦Corresponding author: Li Guo-Fa (Email: lgfseismic@126.com).

Therefore, Wiggins (1978) proposed the minimum entropy deconvolution (MED). Unlike spiking deconvolution, which seeks to whiten the reflectivity spectrum, the MED seeks the smallest number of large spikes that are consistent with the seismic data. As discussed by Sacchi et al. (1994), the above methods are linear approaches to seismic deconvolution, and the ability of these methods to improve the resolution is restricted by the effective frequency band of the seismic data. In other words, obtaining high-frequency components outside the effective frequency band using these deconvolution algorithms is difficult.

To further improve the resolution of seismic data, the sparse-spike deconvolution (SSD) technology with L1 norm constraint has been developed (Taylor et al., 1979; Wang et al., 2016). This method assumes that the Earth's reflectivity can be represented as a superposition of spikes (Gholami and Sacchi, 2012; Zhang and Castagna, 2011) and improves the resolution of seismic records on the basis of the sparse feature of reflection coefficients. Although SSD can improve the resolution of seismic data compared to linear deconvolution, its deconvolution results have inherent multiplicity. However, SSD is based on the 1D forward model, and each seismic trace is processed independently in the SSD algorithm. This means the SSD algorithm does not take into account the spatial correlation that exists in the seismic data, which may result in the poor lateral continuity of the deconvolved results. To take full advantage of the inherent spatial continuity of the seismic traces, some scholars have proposed many deconvolution methods by using multichannel inversion scheme (Zhang et al., 2013; Gholami and Sacchi, 2013; Kazemi and Sacchi, 2014; Wang and Wang, 2017; Ma et al., 2017; Du et al., 2018; Ma et al., 2020a,b,c). Among them, Gholami and Sacchi (2013) used multichannel reflectivity inversion with total variation regularization, which can obtain relatively good results when the underground structure is simple (Gholami and Sacchi, 2012). Du et al. (2018) proposed a dip-constrained multichannel deconvolution algorithm, which introduces seismic dip information into the multichannel deconvolution algorithm for situations where seismic dips change greatly. However, the actual seismic structure cannot be characterized simply by the seismic dips. To better exert the spatial constraint effect on the deconvolution result, we propose structurally constrained deconvolution (SCD) using spatial reflection regularization. Different from total variation regularization and dip regularization methods, this method uses *t-x* prediction-error filter (PEF), which was introduced by Claerbout (1992), to characterize the continuity and spatial structure of seismic signals. The *t-x* PEF is applied to construct the structural regularization term for accounting for the spatial connection between seismic traces. The effectiveness of this approach is demonstrated by using both synthetic data and field examples.

The structure of this paper is as follows: First, we briefly review the principle of SSD. Then, we construct a spatial reflection regularization by using *t-x* PEF. Next, we incorporate the spatial reflection regularization into the deconvolution algorithm and develop the SCD algorithm. After that, we apply synthetic and field data examples to demonstrate the effectiveness of the proposed method. Finally, we draw some conclusions.

Theory and method

Sparse-spike deconvolution

On the basis of the 1D forward model, the seismic data can be modeled by convolving the reflectivity series with a source wavelet (Yilmaz, 2001)

$$d(t) = w(t) * r(t), \tag{1}$$

where the notation * denotes the convolution, $d(t)$ is the seismogram, $w(t)$ is the band-limited wavelet, and $r(t)$ is the reflectivity sequences. The matrix-vector form of equation (1) can be expressed as

$$\mathbf{d} = \mathbf{W}\mathbf{r}, \tag{2}$$

where vectors **d** and **r** are the discrete representations of the seismogram and reflectivity, respectively; and the matrix **W** is a square Toeplitz matrix that corresponds to the source wavelet w. An illustration of the 1D convolutional model is shown in Figure 1.

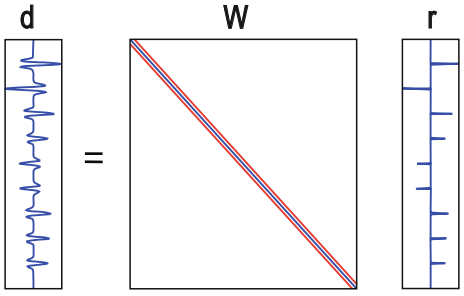

Fig. 1. Illustration of the 1D convolutional model. The algebraic notations d, W, and r are the synthetic seismic trace, the Ricker wavelet matrix, and the reflectivity sequences, respectively.

With the assumption that the reflectivity is a sparse sequence of spikes, seismic deconvolution is, therefore, about solving a sparse recovery problem. Many SSD algorithms are developed by imposing sparseness regularization on the reconstructed reflectivity sequences. In this paper, we use the L1 norm to constrain the reflectivity and set up the following objective function (Taylor et al., 1979):

$$\phi(\mathbf{r}) = \frac{1}{2}\|\mathbf{W}\mathbf{r} - \mathbf{d}\|_2^2 + \lambda\|\mathbf{r}\|_1, \tag{3}$$

where $\lambda \in (0,\infty)$ is a tradeoff parameter that can be chosen by the cross-validation criterion.

We choose the alternating direction method of multipliers (ADMM) to solve this $L1$-regularized problem. The approach of the ADMM formula is to decouple the cost function into a quadratic term and $L1$ norm term, which can be expressed as (Boyd et al., 2011)

$$\min_{\mathbf{r},\mathbf{z}} f(\mathbf{r}) + g(\mathbf{z}) \quad s.t. \quad \mathbf{r} - \mathbf{z} = \mathbf{0}, \tag{4}$$

where $\mathbf{z}$ is an auxiliary variable, $f(\mathbf{r}) = \frac{1}{2}\|\mathbf{W}\mathbf{r} - \mathbf{d}\|_2^2$, and $g(\mathbf{z}) = \lambda\|\mathbf{z}\|_1$. We then form the augmented Lagrangian

$$L_\rho(\mathbf{r},\mathbf{z},\mathbf{u}) = f(\mathbf{r}) + g(\mathbf{z}) + \mathbf{u}^T(\mathbf{r} - \mathbf{z}) + \frac{\rho}{2}\|\mathbf{r} - \mathbf{z}\|_2^2, \tag{5}$$

where $\mathbf{u}$ is the Lagrange multiplier, and ρ is a penalty parameter.

The unscaled-form ADMM consists of the iterations (Boyd et al., 2011)

$$\begin{cases} \mathbf{r}^{k+1} = \min\limits_{\mathbf{r}} L_\rho(\mathbf{r},\mathbf{z}^k,\mathbf{u}^k) = (\mathbf{W}^T\mathbf{W} + \rho\mathbf{I})^{-1}(\mathbf{W}^T\mathbf{d} + \rho\mathbf{z}^k - \mathbf{u}^k) \\ \mathbf{z}^{k+1} = \min\limits_{\mathbf{z}} L_\rho(\mathbf{r}^{k+1},\mathbf{z},\mathbf{u}^k) = S(\mathbf{r}^{k+1} + \mathbf{u}^k, \lambda/\rho) \\ \mathbf{u}^{k+1} = \mathbf{u}^k + \rho(\mathbf{r}^{k+1} - \mathbf{z}^{k+1}) \end{cases}, \tag{6}$$

where k is the index of iteration. The $\mathbf{r}$-update step is quadratic, and its solution is simply obtained by setting its derivative with respect to $\mathbf{r}$ equals zero. The $\mathbf{z}$-update step can be solved using a soft-thresholding algorithm with the operator

$$S(\mathbf{r},\gamma) = sgn(\mathbf{r})max\{|\mathbf{r}| - \gamma, 0\}, \tag{7}$$

where $sgn(*)$ is a sign function and γ denotes the threshold value. The $\mathbf{u}$-update can be calculated in a straightforward manner.

The stopping criterion for the ADMM algorithm is

$$\left(\frac{\|\mathbf{r}^{k+1} - \mathbf{r}^k\|_2}{\max\left\{\|\mathbf{r}^{k+1}\|_2, \|\mathbf{r}^k\|_2\right\}} \le \varepsilon \right) \cup (k > N), \tag{8}$$

where $\varepsilon > 0$ is a given tolerance, and N is the maximum number of iterations.

Constructing a spatial reflection constraint

SSD is based on the 1D convolution model [equation (2)], and each seismic trace is processed independently. Thus, the deconvolved results may show poor spatial continuity when the input seismic data are contaminated by seismic noise. To address this issue, we extend the 1D forward model to a multichannel forward system and then use the spatial constraint to ensure the lateral continuity of deconvolved results.

When considering a 2D seismic profile, we can generalize the 1D convolution model [equation (2)] to a multichannel system (Du et al., 2018)

$$\underbrace{\begin{bmatrix} \mathbf{d}_1 \\ \mathbf{d}_2 \\ \vdots \\ \mathbf{d}_M \end{bmatrix}}_{\mathbf{s}} = \underbrace{\begin{bmatrix} \mathbf{W}_1 & \mathbf{0} & \mathbf{0} & \mathbf{0} \\ \mathbf{0} & \mathbf{W}_2 & \mathbf{0} & \mathbf{0} \\ \mathbf{0} & \mathbf{0} & \ddots & \mathbf{0} \\ \mathbf{0} & \mathbf{0} & \mathbf{0} & \mathbf{W}_M \end{bmatrix}}_{\mathbf{G}} \underbrace{\begin{bmatrix} \mathbf{r}_1 \\ \mathbf{r}_2 \\ \vdots \\ \mathbf{r}_M \end{bmatrix}}_{\mathbf{m}}, \tag{9}$$

where s and $\mathbf{m}$ are the concatenated vector of 2D seismic data and reflectivity model, respectively; and $\mathbf{G}$ is a block diagonal matrix with $\mathbf{W}$ as its element. An example of a multichannel convolution model for generating four seismic traces simultaneously is shown in Figure 2.

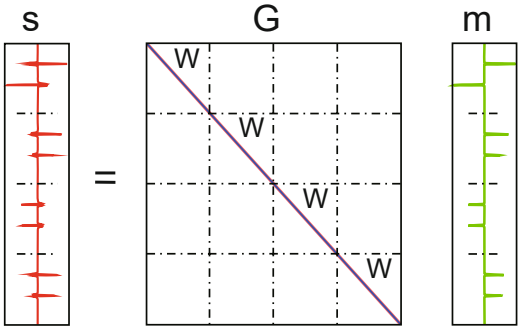

Fig. 2. Multichannel forward system for generating four seismic traces simultaneously. The algebraic notations s, G, and m are the concatenated seismic data, the block Ricker wavelet matrix, and the concatenated reflectivity model, respectively.

To protect the lateral continuity of the deconvolved

results, we should extract the spatial coherency information in the seismic data. As discussed by Claerbout (1992), *t*-*x* PEF is a useful tool to account for the spatial connection between seismic traces (Fomel, 2002). In 2D cases, the PEF with 20 prediction coefficients can be defined as (Abma and Claerbout, 1995; Ma et al., 2020c)

$$\begin{matrix} h_{-2,-2} & h_{-2,-1} & 0 & h_{-2,1} & h_{-2,2} \\ h_{-1,-2} & h_{-1,-1} & 0 & h_{-1,1} & h_{-1,2} \\ h_{0,-2} & h_{0,-1} & -1 & h_{0,1} & h_{0,2} \\ h_{1,-2} & h_{1,-1} & 0 & h_{1,1} & h_{1,2} \\ h_{2,-2} & h_{2,-1} & 0 & h_{2,1} & h_{2,2} \end{matrix}, \tag{10}$$

where the vertical and horizontal axes are the time and space axes, respectively. The output position is at the center of the filters (marked by–1).

T–*x* PEF can be calculated by minimizing the following functional (Liu et al., 2015):

$$\phi(h_{i,j}) = \left\| d(t,x) - \sum_{j=-2, j\neq 0}^{2} \sum_{i=-2}^{2} h_{i,j} d_{i,j}(t,x) \right\|_2^2, \tag{11}$$

where $d_{i,j}(t,x)$ represents the translation of the raw seismic data $d(t,x)$ in the time and space directions with time shift i and space shift j. This problem [equation (11)] is quadratic, and we can solve it using a conjugate gradient algorithm.

After obtaining *t*-*x* PEF, we can estimate the prediction errors by the following 2D convolution (Ma et al., 2020c):

$$e(t,\ x) = h_{i,j} * m(t,\ x),\ \ i, j = -2,\ -1,\ 0,\ 1,\ 2, \tag{12}$$

where $e(t,x)$ is the prediction error at each position, and $m(t,x)$ is the required retrieved model parameter (e.g., the reflectivity model). If the raw seismic data $d(t,x)$ and the retrieved model $m(t,x)$ have a similar seismic reflection structure, then the prediction errors $e(t,x)$ should be small. In contrast, if they are dissimilar, then the prediction errors are bigger. This means $t - x$ PEF quantitatively describes the reflection structure differences between two seismic data.

Equation (12) is a 2D convolution problem that is difficult to solve. According to Claerbout (1998), we can employ the helix transform to transform it into 1D space, which is expressed as

$$e_{1d} = h_{1d} * m_{1d}, \ \text{ or } \ \mathbf{e} = \mathbf{Hm}, \tag{13}$$

where $\mathbf{H}$ is a convolution matrix constructed by PEF.

Generally, the low-frequency seismic data $d(t,x)$ and the required reflectivity model are inherently different, which may reduce the accuracy of the spatial reflection constraint. To improve its reliability, we construct the spatial reflection constraint by applying a low-pass filter to the retrieved reflectivity sequences

$$\phi(\mathbf{m}) = \left\| \mathbf{HLm} \right\|_2^2, \tag{14}$$

where $\mathbf{L}$ is a low-pass filter operator. The selection of the low-pass filter operator needs to be estimated based on the dominant frequency band of the field data. Generally, the highest frequency of the dominant frequency band can be expanded by two times, which is the highest frequency of the low-pass filter.

Multichannel deconvolution with a spatial reflection constraint

To constrain the spatial continuity of the inverted results, we incorporate the spatial reflection constraint term [equation (14)] into the framework of the multichannel inversion to establish the following objective function:

$$\phi(\mathbf{m}) = \frac{1}{2}\left\| \mathbf{Gm - s} \right\|_2^2 + \lambda_z \left\| \mathbf{m} \right\|_1 + \frac{\lambda_x}{2}\left\| \mathbf{HLm} \right\|_2^2, \tag{15}$$

where λ_x is the regularization parameter that controls the relative strength of the vertical constraint, and λ_x is the regularization parameter that controls the relative strength of the spatial reflection constraint item.

We adopt the ADMM algorithm to minimize the above objective function (equation (15)). With the introduction of an auxiliary variable $\mathbf{z}$, equation (15) can be converted to the following minimization problem:

$$\begin{aligned} \phi(\mathbf{m}, \mathbf{z}) = \frac{1}{2}\left\| \mathbf{Gm} - \mathbf{s} \right\|_2^2 + \lambda_z \left\| \mathbf{z} \right\|_1 + \frac{\lambda_x}{2}\left\| \mathbf{HLm} \right\|_2^2 \\ \text{s.t. } \ \mathbf{m} - \mathbf{z} = \mathbf{0}. \end{aligned} \tag{16}$$

The augmented Lagrangian formula of equation (16) is then written as

$$\begin{aligned} L(\mathbf{m}, \mathbf{z}, \mathbf{y}) = \frac{1}{2}\left\| \mathbf{Gm} - \mathbf{s} \right\|_2^2 + \lambda_z \left\| \mathbf{z} \right\|_1 \\ + \frac{\lambda_x}{2}\left\| \mathbf{HLm} \right\|_2^2 + \frac{\mu}{2}\left\| \mathbf{m} - \mathbf{z} + \mathbf{y} \right\|_2^2, \end{aligned} \tag{17}$$

where the vector $\mathbf{y}$ is the Lagrangian multiplier, and μ is the regularization parameter.

Equation (17) can be minimized by decomposing it into the following subproblems:

$$\begin{cases} \mathbf{m}^{k+1} = \min\limits_{\mathbf{m}} L(\mathbf{m}, \mathbf{z}^k, \mathbf{y}^k) \\ \mathbf{z}^{k+1} = \min\limits_{\mathbf{z}} L(\mathbf{m}^{k+1}, \mathbf{z}, \mathbf{y}^k) \\ \mathbf{y}^{k+1} = \mathbf{y}^k + \mathbf{m}^{k+1} - \mathbf{z}^{k+1} \end{cases}, \tag{18}$$

or

$$\begin{cases} \mathbf{m}^{k+1} = \left[\mathbf{G}^T\mathbf{G} + \lambda_x(\mathbf{HL})^T(\mathbf{HL}) + \mu\mathbf{I}\right]^{-1}(\mathbf{G}^T\mathbf{s} + \mu\mathbf{z}^k - \mu\mathbf{y}^k) \\ \mathbf{z}^{k+1} = S(\mathbf{m}^{k+1} + \mathbf{y}^k, \lambda_z/\mu) \\ \mathbf{y}^{k+1} = \mathbf{y}^k + \mathbf{m}^{k+1} - \mathbf{z}^{k+1} \end{cases}. \tag{19}$$

The proposed deconvolution algorithm includes a spatial reflection constraint; thus, we refer to it as SCD algorithm.

In this algorithm, the regularization parameters λ_z, λ_x, and have a greater impact on the deconvolution effect and are not easy to select. Therefore, we give the empirical selection range of the regularization parameters here. The regularization parameter λ_z generally accepts a value of 0.01–1. When the signal-to-noise ratio is high, the value λ_z can be small to improve the vertical resolution of the deconvolution result; when the signal-to-noise ratio is low, the value of should be large to suppress the amplification of noise. The value λ_x generally changes with the value λ_z, and the initial value of λ_x can generally be set to λ_z. If the lateral continuity of the deconvolution result at this time is poor, then the value λ_x can be increased between 10 and 100 times. If the deconvolution result at this time is already good, then the value λ_x can be adjusted in the same order of magnitude. The selection strategy of the regularization parameter is similar to the parameter λ_x, and both of them treat λ_z as a reference.

Example

Synthetic experiments

In this section, we investigate the superior performance of the proposed SCD algorithm compared to that of the SSD approach. In the first experiment, simple synthetic data containing flat and dip events are used and shown in Figure 3(a). Figure 3(b) presents noisy seismic data with 40% Gaussian noise. We use both the SCD and SSD methods to process the noisy data, and their corresponding results are shown in Figures 3(c) and 3(d), respectively. As demonstrated in Figure 3(c), the result obtained by the SSD approach is noisy and laterally discontinuous. In contrast, the proposed SCD method provides a reflectivity profile with improved noise reduction and lateral continuity.

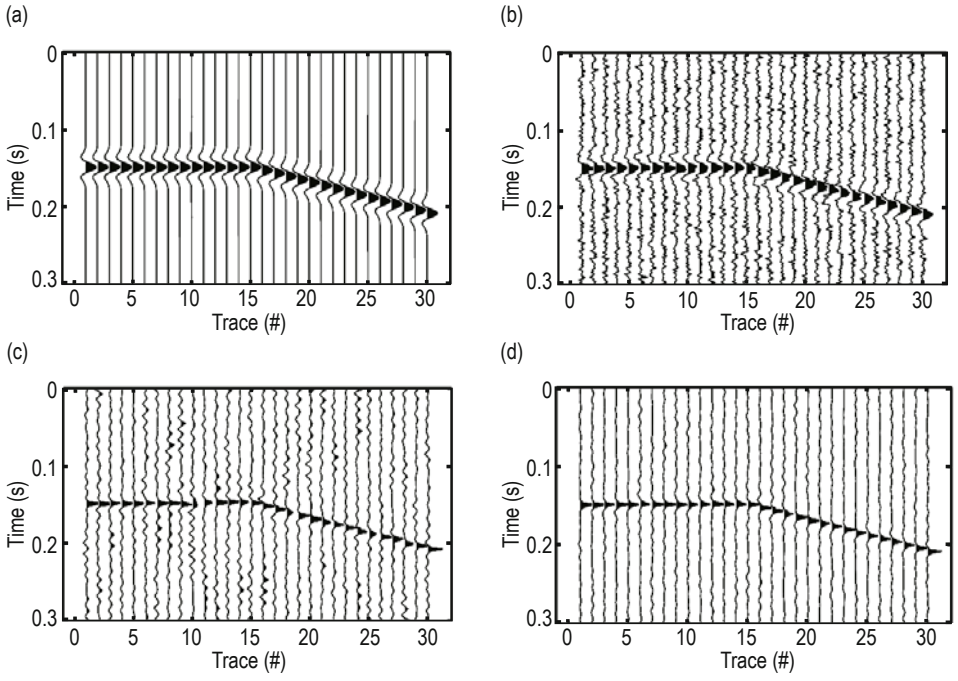

Fig. 3. Simple deconvolution test. (a) The synthetic data containing flat and dip events, (b) the noisy seismic data with 40% Gaussian noise, (c) the result obtained by the SSD approach, and (d) the result obtained by the SCD approach.

Multichannel deconvolution

To further demonstrate the superiority of the SCD algorithm compared to the SSD method, we apply relatively complex synthetic data in the second test. Figure 4a shows the reflectivity model used to generate the synthetic seismic data. In this experiment, we choose a 30 Hz Ricker wavelet as the source wavelet. Convolving this source wavelet with the above reflectivity model, we obtain the noise-free synthetic data (Figure 4b). Figure 4c displays the noisy seismic data with 30% random noise, which is used to conduct the deconvolution tests.

To enhance the resolution of the raw data, we use both the SCD and SSD methods to process the noisy data. In the SSD algorithm, we choose the regularization parameter λ_z=0.04 by trial and error. The corresponding deconvolution result is displayed in Figure 5a. In the SCD method, we fix the parameter λ_z=0.04 and select a lateral regularization parameter λ_x=1 by trial and error. The reconstructed reflectivity is shown in Figure 5b. As shown in Figure 5, both methods evidently improve the seismic resolution of raw data. However, compared with the SSD result, the SCD result has better spatial continuity and higher S/N ratio, which indicates the effectiveness and superiority of the proposed SCD method in suppressing random noise and preserving the spatial continuity.

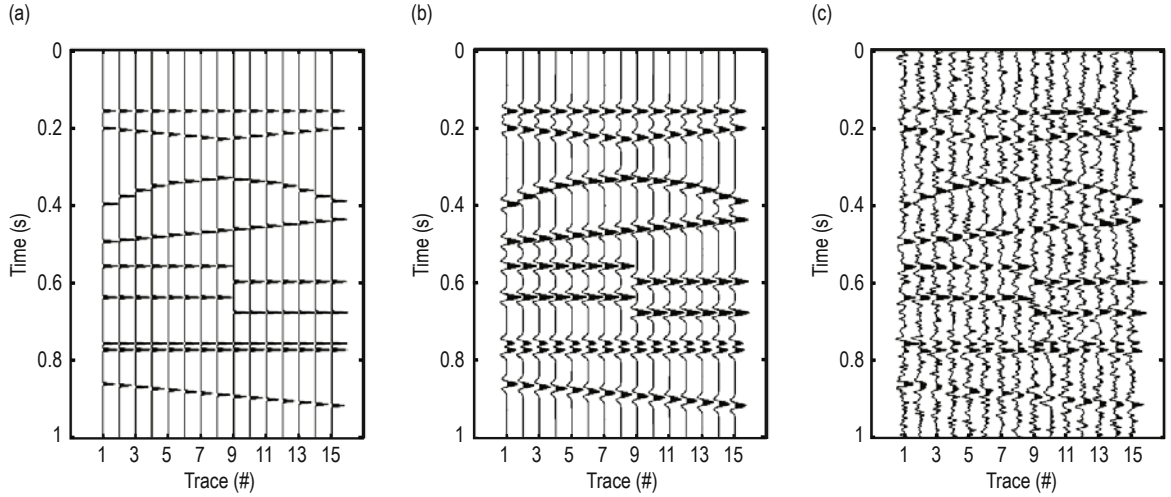

Fig. 4. Forward modeling for generating the synthetic data. (a) The reflectivity model, (b) the noise-free synthetic data, (c) the noisy data with 30% Gaussian noise.

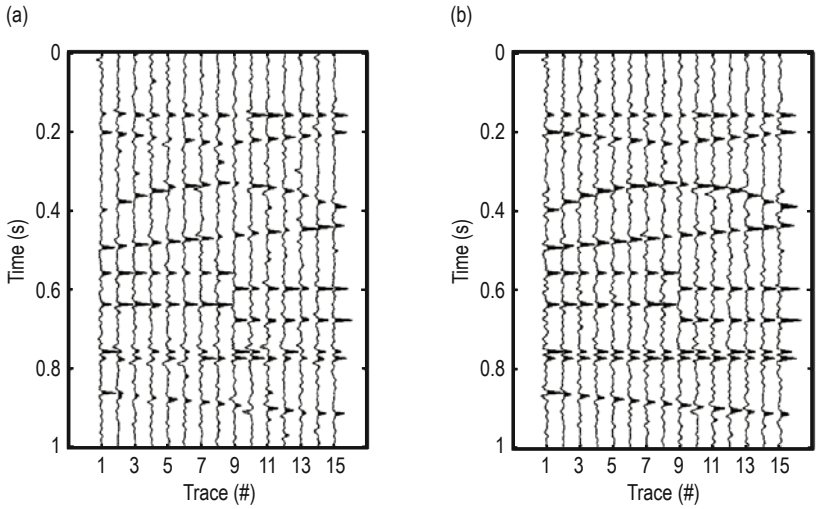

Fig. 5. Deconvolution results processed by using (a) the SSD algorithm and (b) the SCD algorithm.

We also use the average correlation coefficient (ACC) to quantitatively measure the deconvolution accuracy of both methods. The ACC is defined as

$$ACC = \frac{1}{M}\sum_{i=1}^{M}\frac{\mathbf{x}_i^T\mathbf{y}_i}{\|\mathbf{x}_i\|_2\|\mathbf{y}_i\|_2}, \tag{20}$$

where M is the trace number, and x_i and y_i are the referenced and deconvolved seismic traces, respectively. The ACC between the SSD result and the ideal data is 0.74, and the ACC between the SCD result and the reference reaches 0.83, which further indicates that the proposed method has better accuracy than the SSD algorithm.

Figure 6 shows the amplitude spectra of the original data (red), that of the SSD result (blue), and the SCD result (green). Both algorithms broaden the bandwidth of the raw data, and the frequency content of the deconvolution data is analogous. The small difference between the SSD and SCD may result from the suppression of seismic noise.

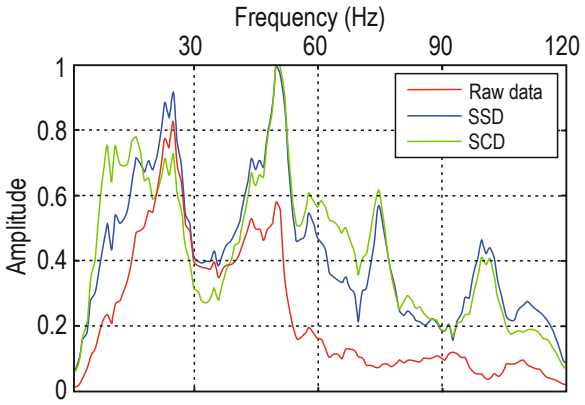

Fig. 6. Amplitude spectra of the original data (red), that of the SSD result (blue), and that of the SCD result (green).

Real data tests

To demonstrate the practicability of the proposed SCD algorithm in field data, we utilize the seismic data shown in Figure 7 to conduct the deconvolution test. To enhance the resolution of raw seismic data, we process the seismic section by performing the following four steps: First, we estimate a zero-phase seismic wavelet by using spectral simulation technology (Lines and Ulrych, 1977). Then, we calculate the t − x PEF from the raw data, which are the required inputs to constrain the lateral continuity.

Next, we find that the dominant bandwidth of the raw data is approximately 5–60 Hz, and we design a 1–5–100–120 Hz band-pass filter to construct the operator **L** in the cost function of the SCD algorithm. Lastly, we use both SSD and SCD algorithms to process the raw data.

In the SSD algorithm, the raw data are processed trace-by-trace, and the recovered reflectivity result is shown in Figure 8. The deconvolved section reveals an evident improvement in the vertical resolution but suffers from a lack of lateral continuity (see arrows). In the SCD algorithm, we take the spatial correlation of seismic traces into consideration, and the inverted result is shown in Figure 9. By comparing these two reconstructed reflectivity profiles, we find that both algorithms have a similar ability in improving seismic resolution, but the result of the proposed SCD method exhibits improved lateral continuity (see the seismic events marked by arrows). Figure 10 shows the amplitude spectra of the raw data (red), that of the SSD result (blue), and that

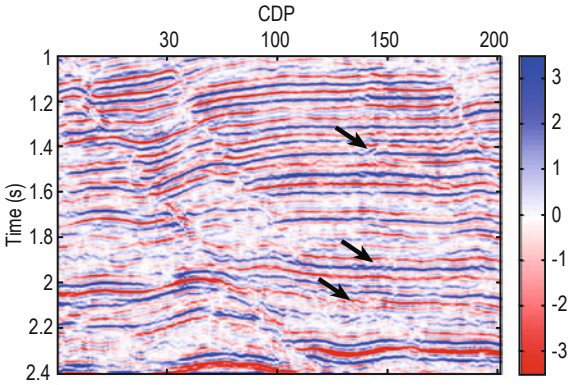

Fig. 8. Deconvolution result using the SSD algorithm.

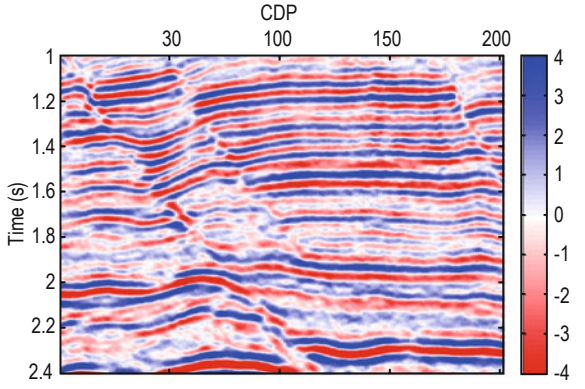

Fig. 7. Field data before seismic deconvolution.

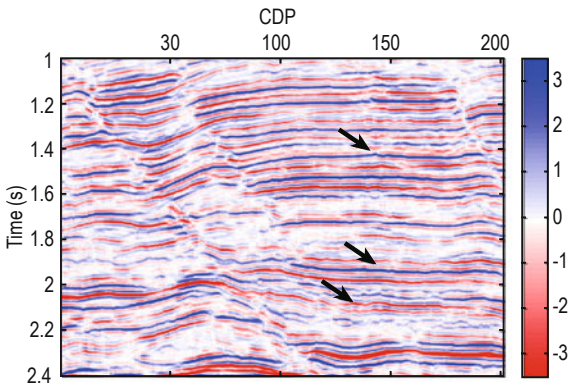

Fig. 9. Deconvolution result using the SCD algorithm.

of the SCD result (green). From the amplitude spectra, we observe that both methods evidently extend the bandwidth of the raw data, and a small difference exists between the spectra of the SSD and that of the SCD.

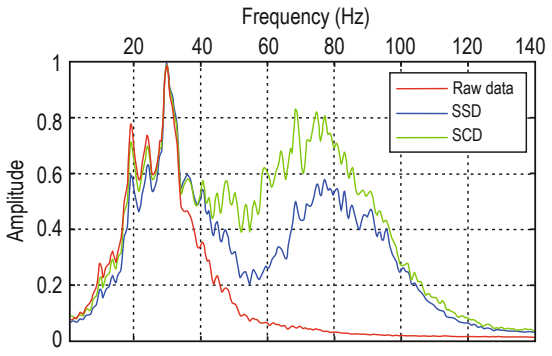

Fig. 10. Amplitude spectra of the field data (red), that of the SSD result (blue), and that of the SCD result (green).

Conclusions

We proposed a SCD method by introducing spatial reflection regularization into the deconvolution algorithm. *t-x* PEF is the key component in constructing the spatial reflection constraint. In the cost function of the algorithm, we utilize not only the sparse reflectivity regularization in the vertical direction, but also the continuity constraint in the spatial direction. This three-term cost function is then efficiently solved by ADMM. Benefiting from the introduction of spatial constraint, the proposed SCD approach can provide a deconvolution result with high resolution and improved spatial continuity. The synthetic and field data tests demonstrate that the proposed SCD method can effectively enhance seismic vertical resolution without losing spatial continuity.

Acknowledgments

We are grateful to the anonymous reviewers and the editor for their constructive comments and suggestions, which have helped improve the logic of this paper.

References

Abma, R., and J. Claerbout, 1995, Lateral prediction for noise attenuation by t-x and f-x techniques: Geophysics, **60**, 1887–1896.

Berkhout, A. J., 1977, Least-squares inverse filtering and wavelet deconvolution: Geophysics, **42**, 1369–1383.

Boyd, S., N. Parikh, E. Chu, B. Peleato, and J. Eckstein, 2011, Distributed optimization and statistical learning via the alternating direction method of multipliers: Foundations and Trends in Machine Learning, **3**, 1–122.

Claerbout, J. F., 1992, Earth soundings analysis: Processing versus inversion: Blackwell Scientific Publications.

———, 1998, Multidimensional recursive filters via a helix: Geophysics, **63**, 1532–1541.

de Figueiredo, L. P., M. Santos, M. Roisenberg, G. S. Neto, and W. Figueiredo, 2014, Bayesian framework to wavelet estimation and linearized acoustic inversion: IEEE Geoscience and Remote Sensing Letters, **11**, 2130–2134.

Du, X., G. Li, M. Zhang, H. Li, W. Yang, and W. Wang, 2018, Multichannel band- controlled deconvolution based on a data-driven structural regularization: Geophysics, **83**, R401–R411.

Fomel, S., 2002, Applications of plane-wave destructor filters: Geophysics, **67**, 1946–1960.

Gholami, A., and M. D. Sacchi, 2012, A fast and automatic sparse deconvolution in the presence of outliers: IEEE Transactions on Geoscience and Remote Sensing, **50**, 4105–4116.

Gholami, A., and M. D. Sacchi, 2013, Fast 3D blind seismic deconvolution via constrained total variation and GCV: SIAM Journal on Imaging Sciences, **6**, 2350–2369.

Kazemi, N., and M. D. Sacchi, 2014, Sparse multichannel blind deconvolution: Geophysics,**79**, V143–V152.

Li, L., 2014, Sparsity-promoted blind deconvolution of ground-penetrating radar (GPR) data: IEEE Geoscience and Remote Sensing Letters, **11**, 1330–1334.

Lines, L. R., and T. J. Ulrych, 1977, The old and the new in seismic deconvolution and wavelet estimation: Geophysical Prospecting, **25**, 512–540.

Liu, Y., N. Liu, and C. Liu, 2015, Adaptive prediction filtering in t-x-y domain for random noise attenuation using regularized nonstationary autoregression: Geophysics, **80**, V13–V21.

Ma, M., S. Wang, S. Yuan, J. Wang, and J. Wen, 2017, Multichannel spatially correlated reflectivity inversion

using block Sparse Bayesian Learning: Geophysics, **82**, V191– V199.

Ma, X., G. Li, S. He, H. Li, and Z. Wang, 2020a, Spatially constrained attenuation compensation in the mixed domain: Geophysical Prospecting, **68**, 1819–1833.

Ma, X., G. Li, H. Li, J. Li, and X. Fan, 2020b, Stable absorption compensation with lateral constraint: Acta Geophysica, **68**, 1039–1048.

Ma, X., G. Li, H. Li, and W. Yang, 2020c, Multichannel absorption compensation with a data-driven structural regularization: Geophysics, **85**, V71–V80.

Sacchi, M. D., D. R. Velis, and A. H. Cominguez, 1994, Minimum entropy deconvolution with frequency-domain constraints: Geophysics, **59**, 938–945.

Taylor, H. L., S. C. Banks, and J. F. McCoy, 1979, Deconvolution with the L1 norm: Geophysics, **44**, 39–52.

Wang, L., Q. Zhao, J. Gao, Z. Xu, M. Fehler, and X. Jiang, 2016, Seismic sparse-spike deconvolution via Toeplitz-sparse matrix factorization: Geophysics, **81**, V169–V182.

Wang, R., and Y. Wang, 2017, Multichannel algorithms for seismic reflectivity inversion: Journal of Geophysics and Engineering, **14**, 41–50.

Wiggins, R. A., 1978, Minimum entropy deconvolution: Geoexploration, **16**, 21–35.

Yilmaz, O., 2001, Seismic Data Analysis: Society of Exploration Geophysicists.

Zhang, R., and J. Castagna, 2011, Seismic sparse-layerreflectivity inversion using basis pursuit decomposition: Geophysics, **76**, R147–R158.

Zhang, R., M. K. Sen, and S. Srinivasan, 2013, Multi-trace basis pursuit inversion with spatial regularization: Journal of Geophysics and Engineering, **10**, 035012.

Li Hao, he earned his master's degree (i 2012) in geological engineering (geophysical exploration) from the China University of Petroleum (Beijing). Now he is studying his PhD in College of Geophysics of the university. His research interests are high-resolution seismic data processing and complex reservoir prediction methods